



**HAL**  
open science

## Acoustics and petrophysical investigations on upper cretaceous carbonate rocks from northern Lebanon

Mohamed K. Salah, Mohammad Alqudah, Christian David

► **To cite this version:**

Mohamed K. Salah, Mohammad Alqudah, Christian David. Acoustics and petrophysical investigations on upper cretaceous carbonate rocks from northern Lebanon. *Journal of African Earth Sciences*, 2020, 172, pp.103955. 10.1016/j.jafrearsci.2020.103955 . hal-03478992

**HAL Id: hal-03478992**

**<https://hal.science/hal-03478992>**

Submitted on 5 Apr 2022

**HAL** is a multi-disciplinary open access archive for the deposit and dissemination of scientific research documents, whether they are published or not. The documents may come from teaching and research institutions in France or abroad, or from public or private research centers.

L'archive ouverte pluridisciplinaire **HAL**, est destinée au dépôt et à la diffusion de documents scientifiques de niveau recherche, publiés ou non, émanant des établissements d'enseignement et de recherche français ou étrangers, des laboratoires publics ou privés.

# **Acoustics and Petrophysical Investigations on Upper Cretaceous Carbonate Rocks from Northern Lebanon**

**Mohamed K. Salah<sup>1\*</sup>, Mohammad Alqudah<sup>2</sup>, Christian David<sup>3</sup>**

<sup>1</sup> Department of Geology, American University of Beirut, Riad El Solh 1107 2020, Beirut, Lebanon

<sup>2</sup> Earth and Environment Sciences Department, Faculty of Science, Yarmouk University, 21163 Irbid, Jordan

<sup>3</sup> Dept. Geosciences & Environment, CY Cergy Paris Université, F-95031, Cergy-Pontoise, France

\*Corresponding Author: Mohamed K. Salah; E-Mail: [ms264@aub.edu.lb](mailto:ms264@aub.edu.lb)

## **Abstract**

Carbonate rocks represent significant aquifers and reservoir rocks in many parts of the world. In this study, twenty-one carbonate samples collected from the exposed rocks at Batroun and Chekka, northwestern Lebanon, are studied to investigate their lithological characteristics, nannofossil content, and their acoustic and petrophysical properties. Four microfacies are recognized in the studied rocks including packstone, wackstone, wack-mudstone, and the wack-packstone. Nannofossils are detected in the top part of the studied section indicating marine-type depositional conditions for the upper Cretaceous carbonate rocks. The Petrographic analysis revealed also that the studied rocks have moderate to high porosity which is consistent with the measured porosity on core samples. The low porosity of some samples is induced by cementation, which also reduced their permeability. The bulk density varies widely because of the many diagenetic processes that impacted the studied rocks. Moreover, because the primary and secondary wave velocities ( $V_p$ , and  $V_s$ ) are greatly influenced by porosity and density, the samples exhibit extreme variations in acoustic velocities from low values which characterize soft, highly-porous, rocks to higher velocities

which are characteristic of compact, massive, and highly-cemented carbonates. Some relationships between the measured petrophysical and acoustic parameters are studied to investigate their mutual dependence, and discuss the impacts of rock composition and diagenetic alterations on the petrophysical properties of the collected rocks. The obtained results are also important in characterizing their mechanical strength, and in the analysis of seismic reflection profiles acquired for equivalent offshore limestone reservoirs in the Levant and the Eastern Mediterranean regions.

**Keywords:** Acoustics, Petrophysical Properties; Nannofossils; Chekka Formation; Northern Lebanon.

## **1. Introduction**

Significant hydrocarbon reservoirs of enhanced porosity and permeability, resulting from prolonged diagenesis and karstification of carbonate rocks, are common in many sedimentary basins around the world (Mazzullo and Chilingarian, 1996; Dürrast and Siegesmund, 1999; Jin et al., 2017), including the supergiant oil fields of the Middle East (Nurmi and Standen, 1997). In addition, carbonate rocks represent significant, water-bearing, karst aquifers formed by fracturing and dissolution of limestone, dolomite or magnesite rock (Harmon and Wicks, 2006). Carbonate rocks are also important building stones whose durability is determined mainly by their geological history, petrophysics, strength and elastic characteristics (Cassar, 2016). In comparison to sandstone reservoirs, the exploration of carbonate rocks is challenging due to many intrinsic heterogeneities at various scales of observation and measurement (e.g., Soete et al., 2015). Such heterogeneities result mainly from variable lithology, sedimentary facies, chemistry/mineralogy, complex rock texture, pore geometry and connectivity, as well as subsequent diagenetic modifications (Kerans, 1988; Loucks, 1999, 2001; Loucks and Handford, 1992; Loucks and Mescher, 2001; Jin et al., 2017; Salah et

al., 2020). These various variables affect also their acoustic properties and the relationships between various reservoir parameters (Neto et al., 2014).

The relationships between acoustic velocities, rock composition, and texture are fundamental to the understanding of sonic logs and seismic reflection profiles of sedimentary basins (e.g., Buckley et al., 2013; Soete et al., 2015). Acoustic impedance, an important rock parameter in reflection seismology, is calculated from the primary wave velocity ( $V_p$ ) and the bulk density ( $\rho_b$ ). Moreover, knowledge of both rigidity and incompressibility of a dry rock is fundamental for the shear wave velocity ( $V_s$ ) prediction and fluid substitution (Neto et al., 2014). The Poisson's ratio ( $\nu$ ) is very sensitive to the presence of fluids, and is widely used in seismic exploration as a lithological gauge (Kearey et al., 2002). In addition to porosity and lithology, these elastic parameters are controlled also by the geometry of pores as well as their connectivity (Li and Zhang, 2011).

Carbonate rocks exhibit very wide ranges in their petrophysical and elastic properties (e.g., Anselmetti and Eberli, 1993, 2001). They are composed essentially of calcite with its well-known matrix density, which implies that other factors control the acoustic wave velocity variations in carbonate rocks. Porosity ( $\phi$ ), which is calculated as the ratio of the volume of the void part of a rock that is unoccupied by rock grains or mineral cement ( $V_{pr}$ ) to the rock's total bulk volume ( $V_b$ ), is the principal parameter affecting the acoustic properties of rocks (e.g., Zolotukhin and Ursin, 2000). It can be divided into primary porosity, secondary porosity, and effective porosity ( $\phi_e$ ). However, results of extensive research done in this field during the last decades indicated that beside porosity, the whole fabric of carbonate rocks controls the variations of acoustic wave velocities (e.g., Wang et al., 1991; Salah et al., 2018). Moreover, their high sensitivity to diagenetic changes may completely modify their porosity, crystal shape, and the rock rigidity (Verwer et al., 2008), which will, in turn, affect their overall elastic properties.

Diagenesis can enhance or diminish significant reservoir properties such as porosity and permeability. The initial porosity of shallow carbonate deposits may be as high as 50-60%. Unlike sandstone reservoirs, subsurface limestone reservoirs have much lower porosities, which decrease gradually with burial depth (Schmoker, 1984; Brown, 1997; Ehrenberg and Nadeau, 2005). Although mechanical compaction is a principal way by which sandstones lose porosity at depths less than about 2.5 km and temperatures of up to 90° C, it is more difficult to assess its effects on carbonates because of the particular grain shape and the high diagenetic potential (Croizé et al., 2010). Meanwhile, if carbonate sediments are not cemented, laboratory investigations revealed that mechanical compaction has the greatest effect on porosity reduction (e.g., Chuhan et al., 2003).

Mineralogically, calcite, aragonite, and dolomite may co-exist in one carbonate rock with varying proportions. These minerals have different stabilities and respond differently to diagenetic processes. The early diagenetic processes may comprise dissolution of unstable components such as aragonite, dolomitization, and the precipitation of low Mg-calcite (Scholle and Halley, 1985). Dissolution, for example, may initially increase the pore volume, while late cementation can either reduce the pore size or result in complete pore closure and, therefore, decreased connectivity, and subsequently low permeability. Early diagenesis may add or remove significant rock constituents in a way that impacts mechanical compaction at shallow burial (e.g., Hamilton, 1976). Shallow platform carbonates, in particular, are very susceptible to early diagenesis (Friedman, 1964), which complicates the prediction of their petrophysical features (e.g., Croizé et al., 2010). Many authors addressed the dominant problems in carbonate petrophysical evaluation resulting from these highly variable rock properties and complex diagenesis (e.g., Lucia, 1999; Akbar et al., 2001; Kennedy, 2002; Cerepi et al., 2003).

The Late Cretaceous carbonate rocks outcropping at Chekka and Batroun areas, northern Lebanon (Fig. 1), which are essentially shallow platform deposits, are selected to study their facies, nannofossil content, and the impact of diagenesis on their petrophysical and elastic characteristics. The obtained results are useful in predicting the rock porosity and elastic properties of the carbonate sediments formed elsewhere at similar conditions, and the respective role of the different diagenetic processes in modifying these parameters. Moreover, the measured parameters including porosity, density, permeability, and the elastic properties are of great importance in characterizing the rocks' mechanical strength and in the analysis of seismic reflection profiles acquired for equivalent offshore limestone reservoirs in the Levant and Eastern Mediterranean regions.

## **2. Geological Setting**

The Lebanese Mesozoic stratigraphic succession is represented mainly by carbonate rocks (Beydoun, 1988; Nader, 2014). The Late Cretaceous beds, in particular, are represented by shallow platform carbonate deposits (Walley, 1983, 1997). During the Late Cretaceous, the Arabian Plate was subject to both compressional and extensional stresses. Compressional stresses resulted in a regional uplift of the Early Turonian up to the Early Campanian during which ophiolitic rocks were obducted at the northeastern and southeastern margins of the Arabian Plate. Extensional stresses in the Coniacian, primarily from the continued opening of the Mediterranean, have possibly affected the northern plate margin as illustrated by the formation of the Euphrates Graben and transgression of the sea in the northwestern side of the Arabian Plate (de Ruiter et al., 1995; Litak et al., 1998). During these extensional regimes, the carbonate platform was formed at the northwestern part of the Arabian Plate. More details on the nature of the depositional conditions and the Mesozoic sediment characteristics in Lebanon can be found in other published works (e.g., Beydoun, 1988; Walley, 1997; Nader, 2014).

### **3. Material and Methods**

We collected a total of twenty-one representative rock samples from the exposed Late Cretaceous rocks at Chekka and Batroun (Fig. 2). These rocks have been studied petrographically and petrophysically as explained in the following paragraphs.

#### ***3.1. Petrography***

The exposed Late Cretaceous Chekka and Batroun rocks at northern Lebanon, and the location of the collected samples are shown in Fig. 3. The petrographic and Scanning Electron Microscopic (SEM) investigations have been carried out to determine the rock facies and the dominant pore types. A total of twenty-one thin sections were analyzed using the polarized microscope to characterize lithology and find out the paleo-environmental depositional conditions. Special attention was paid to evaluate the overall rock porosity, detect the primary and secondary porosities, and to investigate the different post-depositional diagenetic processes. Standard types of microfacies are assigned according to Wilson (1975) and Flügel (1982). Porosity and other thin-section derived parameters are characterized in the same way explained in Salah et al. (2018). In addition, the nannofossil content has been analyzed as described by Alqudah et al. (2019).

#### ***3.2. Petrophysical and acoustic measurements***

The petrophysical measurements were conducted on twenty-one, one-inch-diameter, plugs. First, samples were prepared for measurements in the same way described by Freire-Lista et al. (2016). The effective porosity was measured by the saturation method (e.g., Freire-Lista and Fort, 2017; Salah et al., 2020), and calculated according to the following equation:

$$\varphi_e = [(w_s - w_d)/(w_s - w_m)] \quad (1)$$

where  $w_s$ ,  $w_d$ , and  $w_m$  are the saturated, dry, and submerged sample weights. The numerator corresponds to the pore volume whereas the denominator is equivalent to the sample bulk volume.

The bulk density (in  $\text{g/cm}^3$ ), is calculated from the dry sample weight and its bulk volume as follows:

$$\rho_b = w_d / (w_s - w_m) \quad (2)$$

The matrix density ( $\rho_{ma}$ ,  $\text{g/cm}^3$ ), is calculated from the porosity and the  $\rho_b$  using the following simple equation:

$$\phi = 1 - (\rho_b / \rho_{ma}), \text{ and thus } \rho_{ma} = \rho_b / (1 - \phi) \quad (3)$$

Permeability is a measure of the fluid amount transported by a porous medium within the network of its connected pores (e.g., Amyx et al., 1960). For an incompressible fluid and a horizontal flow in the direction of decreasing pressure, permeability ( $K$ ) is defined, according to Darcy's law, as follows:

$$K = \eta QL / A \Delta p \quad (4)$$

where  $\eta$  is viscosity of fluid,  $Q$  is the flow rate,  $L$  is the sample length,  $A$  is the cross-sectional area of the flow, and  $\Delta p$  is the pressure drop across the flow. Permeability was measured for the dry rock samples using nitrogen gas as the flowing fluid. The measured gas permeability is corrected to the equivalent liquid permeability ( $K_L$ ; Klinkenberg, 1941) as described in Salah et al. (2020). A relationship between the values of five gas permeability measurements and the reciprocal of the applied mean pressure across a rock sample is constructed, with the resulting straight line extrapolated to the vertical axis to give the correct  $K_L$  of the rock sample (Fig. 4).

Acoustic wave velocities are measured using the pulse transmission tool (e.g., Birch, 1960) first on the dried plugs. After the core samples were fully saturated with water for porosity determination, the acoustic velocities were measured again. Both  $V_p$  and  $V_s$  measurements were accomplished using Panametrics Pulser-Receiver (Model 5058PR) and an

Agilent DSO-X-2014A Digital Storage Oscilloscope (100 MHz) with a travel time accuracy of 0.01  $\mu$ s. The P- and S-wave transducers are adhered to the core ends with a thin rubber membrane in between. The waveform is displayed on a screen and the first arrival time is picked on a monitor. The measured travel time for the two rubber membranes are subtracted to get the travel time only across the sample; then the acoustic velocity in the core sample ( $V_p$  or  $V_s$ ) is computed as:  $V = h_s/t$ , where  $h_s$  is the sample length as digitally determined by a micrometer.

The elastic moduli can fully describe the mechanical behavior of the rock. The rock rigidity ( $\mu$ ) quantifies the rock resistance to change in shape as a response to the applied shear without any change in volume, whereas the bulk modulus ( $\kappa$ ) measures the incompressibility of rocks. On the other hand, the Young's modulus ( $E$ ) quantifies the rock response to variations in its length under uniaxial pressure (e.g., Yu et al., 2016). These elastic constants are calculated from the measured seismic wave velocity and bulk density as explained in Mavko et al. (2009). The  $v$  ratio is calculated from the  $V_p$  and  $V_s$  as follows:

$$v = [(V_p^2 - 2V_s^2)/2(V_p^2 - V_s^2)] \quad (5)$$

The elastic constants are also calculated using the following relationships (e.g., Russell and Smith, 2007):

$$\mu = \rho_b V_s^2 \quad (6)$$

$$\kappa = \rho_b [V_p^2 - (4/3)V_s^2] \quad (7)$$

$$E = \rho_b V_s^2 [(3V_p^2 - 4V_s^2)/(V_p^2 - V_s^2)] \quad (8)$$

## 4. Results

### 4.1. Petrography and SEM imaging

Four limestone microfacies are recognized in the investigated samples. These are packstone, wackstone, mud-wackstone, and wack-packstone facies (Table 1, Fig. 5). Table 1

includes also the bioclast and non-bioclast ratios, grain types and percentages, etc. The microfacies are assigned based on the [Dunham's \(1962\)](#) classification.

#### A) *Packstone*

This microfacies is detected in samples C1-C4 (Table 1). The samples are characterized generally by the absence of bioclasts, dominance of calcitic interlocking crystal grains (Fig. 5A), and rhombic dolomite (Fig. 5B). Matrix does not exist; instead, a cement represented by the secondary precipitation of CaCO<sub>3</sub> is common. The cement occurs in the form of geodes as a free crystal growth (Fig. 5A). Iron oxides are also observed within the cement. The samples are grain-supported with voids that resulted from high dissolution during post-sedimentological processes (Fig. 5A and B). These processes have affected the porosity partially first by reducing it through the secondary precipitation, and second by enhancing it with new fenestral pores that were created effectively by dolomitization. In accordance with these observations, Cerepi et al. (1999), described the packstone microfacies as having a monomodal pore network with low porosity and low permeability. The notable absence of matrix and signs of intensive diagenesis observed in the samples indicate that the sea level was at minimum at the bottom of the section.

#### B) *Wackstone*

This microfacies, with a matrix of up to 80%, is the most common as it was detected in the majority of the samples: C5 – C10, and C13 – C18 (Table 1). The matrix is mainly calcium carbonate, although a dolomitic matrix was also observed in samples C5 (Fig. 5C) and C6. Non-bioclasts consist mainly of calcite grains (Fig. 5D), whereas bioclastic skeletons of bone fragments (Fig. 5E), spines (Fig. 5F), gastropods (Fig. 5G), ostracods (Fig. 5H), echinoids (Fig. 5I), benthonic and planktonic foraminifera (Fig. 5J) are also detected in the studied samples. Calcareous nannofossils are found in samples C16-C18. These fossil assemblages have wide ranges of preservation from well-preserved (Fig. 5E, G and H), to

those that are poorly-preserved as they were partially destroyed during the reworking and dissolution of calcium carbonates during post-sedimentary processes (Fig. 5F and J). Different kinds of porosity are observed such as the intragranular pores (Fig. 5K) in which the calcium carbonate skeletons were dissolved totally leaving some bird's eye voids. Fractures are also observed in some samples which might be induced by the stresses affecting the sediments. It is clear from the studied samples that most of the fractures are filled with a secondary precipitation of calcium carbonate (Fig. 5L). Cerepi et. al. (1999) described the wackestone microfacies as having a monomodal pore network, with low porosity and low permeability.

#### C) *Wack-Mudstone*

The wack-mudstone microfacies, with dominant calcite matrix (~93%), and scarcity of grains, is found only in two samples (C11 and C12; Table 1). Few calcitic non-biogenic grains (Fig. 5M), and bioclasts such as ostracods exist in the samples which are dominantly matrix-supported. Porosity is observed in two forms: first as intergranular pores within the matrix and, second, as fractures (Fig. 5N), which are sometimes partially filled with calcium carbonate. Cerepi et. al. (1999), characterized the wackestone-mudstone microfacies as having a monomodal pore network, low porosity, and low permeability; features that are consistent with our observations.

#### D) *Wack-Packstone*

This microfacies is detected in the upper part of the section; mainly in samples C19, C20 and C21. Grain content is again high with predominant biogenic skeletons such as ostracods (Fig. 5O), planktonic and benthonic foraminifera (Fig. 5P) and gastropods (Fig. 5Q). Fossils are mostly well-preserved, although some with moderate to poor preservation were also found (Fig. 5R). The percentage of bioclasts is about 30%, whereas the non-biogenic are rare. This microfacies is enriched in calcareous nannofossil assemblages. Porosity is almost

intragranular where voids exist inside the chambers of the organisms (Fig. 5S). However, some pores are filled with the secondary calcium carbonate precipitation; hence reducing the porosity of the rock (Fig. 5T). Existing microfossils and planktonic foraminifera indicate that the sea level reached its maximum at the time of deposition.

#### ***4.2. Calcareous nannofossils and porosity***

Many stratigraphic units are geographically undifferentiated in Lebanon. Therefore, we here consider the calcareous nannofossil content of the studied strata, which provides information on the pore types and their effects on the acoustic and petrophysical characteristics. In carbonate sediments, the grain shape, the intragrain porosity, and sorting have large impacts on the rock porosity (Lucia, 2007).

The lowermost fifteen samples of the section (C1 - C15) are barren whereas various types of nannofossils are detected in samples C16 - C21 (Fig. 6). Examples include *Amphizygus brooksii*, *Predicosphaera cretacea*, *Lapideacassis mariae*, *Tranolithus minimus*, *Tranolithus orionatus*, *Eiffellithus eximius*, *Watznaueria barnesiae*, *Discorhabdus ignotus*, *Zeugrhabdotus* sp., *Rotelapillus laffittei*, *Broinsonia parca*, and *Gartnerago segmentatum*. Following Varol 1991 and Burnett 1998, the occurrence of *Tranolithus minimus*, *Broinsonia parca* and *Eiffellithus eximius* assigns an Early Campanian age for these samples.

Intragranular pores are clearly seen in many samples (Fig. 6; Table 1). The tiny shields of coccolithophores are composed of two parts: the rim, which is an arranged set of microplates of calcium carbonate, and the central area that has many shapes such as closed plates, sieved-shape plates, and open central area. The sieved-shape central area like *Broinsonia parca* includes micro-pores. The same is happening in open central area nannofossils where the micro-porosity is higher and more effective. For instance, cross-shape central area in *Predicosphaera cretacea* created relatively large voids. The existence of clays

in some samples reduces the porosity by filling the space in the central area as in *Amphizygus brooksii* (Fig. 6).

### **4.3. Petrophysical and acoustic properties**

The measured porosity, bulk and matrix densities, the Klinkenberg permeability,  $V_p$ , and  $V_s$  (of both the dry and saturated plugs) as well as the calculated elastic moduli are given in Table 2. Porosity varies widely from 0.02 to 0.34, the bulk density from 1.70 to 2.77 g/cm<sup>3</sup>, and the matrix density from 2.58 to 2.83 g/cm<sup>3</sup>. In contrast, permeability is generally very low and ranges only between 0.004 and 0.075 mD. Although the studied rocks have generally moderate to high porosity (average 0.18), their permeability is very low due to the small size of the majority of the pores and the high percent of non-connected microporosity (Fig. 6).

Wide variations in  $V_p$  and  $V_s$  are encountered even though the averages of  $V_p/V_s$  and the  $v$  ratios are 1.73 and 0.24, respectively. The  $V_p$  varies from 2834 to 6135 m/s, while the  $V_s$  varies from 1605 to 3429 m/s (Table 2). For a given sample, the value of  $V_s$  is, on average, equal to 0.58 of its  $V_p$  value. Samples having the lowest porosity (C2 and C3) have the highest density, the highest  $V_p$ , the highest  $V_s$ , and high  $v$  (Table 2), and in turn, large elastic moduli. The  $v$  is generally low, where only six, out of the studied twenty-one samples, have  $v > 0.25$ . The acoustic impedance varies from 4.8 to 17.0 \* 10<sup>6</sup> kg/m<sup>2</sup>.s, with an average of 9.3 \* 10<sup>6</sup> kg/m<sup>2</sup>.s. In the following paragraphs, we construct some relationships between these different measurements and discuss the effect of the lithological composition and diagenetic processes on the measured parameters.

#### *A) Petrophysical interrelationships*

Porosity is inversely proportional to bulk density with a high correlation coefficient (Fig. 7A) indicating the reliability of our measurements. On the other hand, porosity is directly proportional to permeability although some scatter is clearly observed (Fig. 7B).

Similar to the relationship between porosity and bulk density, the matrix density and porosity are inversely correlated which reflects the effect of lithological composition on porosity (Fig. 7C). The bulk and matrix densities are directly proportional to each other with a good correlation ( $R^2 = 0.83$ ; Fig. 7D). These relationships indicate that dissolution and leaching of some heavier components in the studied rocks are accompanied by an increase in porosity and a corresponding decrease in density.

#### *B) Porosity versus seismic velocities*

The relationships between porosity and both  $V_p$  and  $V_s$  are strongly inverse with high correlation coefficients (Fig. 8A, and B). In addition, at higher porosities ( $> \sim 0.20$ ),  $V_p$  decreases with saturation but increases at low porosity values. There is, however, very little change in  $V_p$  with saturation at moderate porosity ranges (0.08 – 0.20). This behavior of  $V_p$  after saturation is different from the results of Adam et al. (2006); and Croizé et al. (2010), who detected an overall increase of  $V_p$  with saturation. In contrast, there is a marked decrease in  $V_s$  with saturation where almost all the  $V_s$  values of the water-saturated samples are lower than those of the dry rocks. Only one packstone sample, with a porosity of 0.073%, show a higher  $V_s$  after saturation.

The relationship between  $\phi$  and  $v$  seems interesting as it displays different behaviors for the dry and water-saturated samples. In general, the  $v$  increases with saturation and the rate of that increase is larger at higher porosities (Fig. 8C). Higher  $V_p/V_s$  ratios, at saturation, have also been observed by Croizé et al. (2010). For the dry carbonate samples, an inverse relationship is obtained although with a small correlation coefficient. Meanwhile, a weak direct relationship is observed between  $\phi$  and the  $v$  of the water-saturated samples. The relationship between porosity and acoustic impedance (A.I.) is also inverse with a high correlation coefficient (Fig. 8D). The high correlation coefficient ( $R^2=0.94$ ) between the two

parameters is highly significant for the interpretation of subsurface seismic sections and well log analysis of carbonate reservoirs.

### *C) Porosity versus elastic moduli*

All the elastic moduli of the dry and water-saturated samples decrease clearly with the increase of porosity (Table 2). This is also clear from the inverse relationships with the moderate/high correlation coefficients (Fig. 9A-C). The bulk moduli of the dry limestone samples are generally lower than those of the water-saturated carbonate rocks (Fig. 9A), which is attributed to the slight increase in the  $V_p$  of most samples with saturation (Table 2).

### *D) Density versus acoustic velocities*

Acoustic velocities are strongly dependent on bulk density, which is inversely related to porosity. Thus, the bulk density is directly proportional to the acoustic velocities with high correlation coefficients (Fig. 10A). The  $\rho_b$  is a function of both porosity and composition and has a strong impact on the elastic properties of rocks, which explains the strong dependence of the seismic velocities on density. In contrast, the relationship between  $\rho_{ma}$  and acoustic velocities (Fig. 10B) exhibits weaker correlation. These two relationships together indicate the strong impact of porosity on the acoustic characteristics of the investigated samples.

In Table 3, we provide the correlation coefficients ( $r$  values) which relate the different petrophysical and elastic parameters. Porosity is positively correlated with permeability, but negatively correlated with density, acoustic wave velocities, and the elastic moduli of the dry and water-saturated rocks. Except for permeability and the Poisson's ratio of the water-saturated rocks ( $v_{sat}$ ), the bulk density is positively correlated with the elastic properties of the studied samples. In the same way, the matrix density is also positively correlated with the elastic parameters. Permeability is negatively correlated with the elastic parameters even though with low/fair correlation coefficients. The  $v_{sat}$  is negatively weakly correlated with

other elastic parameters. Finally, the acoustic velocities and the elastic moduli are all strongly positively correlated with each other (Table 3).

## **5. Discussion**

### ***5.1. Petrophysical characteristics***

The petrographical investigations revealed that the studied carbonates are classified to wackstones, packstones, wackstone-packstone, and mud-wackstones (Table 1). The grain sizes in these microfacies is very small, usually less than 100  $\mu\text{m}$  (Lucia, 1995, 1999), pointing to the existence of a large proportion of micropores which contribute to the very low permeability (Table 2). Both bulk density and porosity of the studied plugs exhibit large variations (with averages of 2.21  $\text{g}/\text{cm}^3$  and 0.18, respectively) implying variable impacts of sediment nature and the subsequent diagenesis on the measured parameters (e.g., Ehrenberg et al., 2006).

The poro-perm (the porosity-permeability) relationships are very important in reservoir zonation and characterization. In carbonate rocks, these relations are generally poorly-defined especially for continental and shallow platform carbonate deposits formed in thin water films and under constantly-changing temperature and humidity (Soete et al., 2015). Permeability is dependent not only on porosity, but also on grain size, its distribution, and the connectivity of individual pore spaces. Previous estimates revealed that at a certain reservoir porosity of, for example, 0.25, permeability in carbonate rocks varies over four orders of magnitude because of pore complexities (Neto et al., 2014). Meanwhile, some authors (e.g., Lucia, 1995, 2000) derived correlations for specific pore type and grain size relationships. The observed scatter in our poro-perm relationship (Fig. 7B), and the small  $\phi$ -K correlation coefficient (Table 3) confirm the fact that in addition to porosity, other factors including the grain size distribution, pore size, and mud/clay proportion control permeability as well (e.g., El Sayed et al., 2015).

Carbonate rocks with their very complex pore types, initial fabrics, and higher susceptibility to diagenesis (e.g., dissolution, cementation, recrystallization, dolomitization, etc.), possess various pore networks which complicate the poro-perm relationship (Nurmi and Standen, 1997; Laponi et al., 2011; Dewit et al., 2012). This specific nature of carbonate rocks makes it difficult also to understand the relationship between permeability and seismic velocity.

## ***5.2. Pore types and elastic properties of carbonates***

Diversity of pore types in carbonate rocks can produce great changes in seismic velocity at a given porosity (Sun et al., 2006). Soete et al. (2015) found that carbonate rocks with mouldic pores plot above the regression line of the  $\phi$ - $V_p$  relationship compared to those with micro-moldic porosity, which plot well below the regression line. In addition, samples with vugs appear close to, and around, the best-fit line, whereas those of framework porosity have lower velocities and plot below the average trend.

In our study, some samples on the porosity-velocity show different porosities at close velocities and different velocities at similar porosities (Fig. 8A and B). According to previous studies, these discrepancies arise from the complex pore system, where an increase in the percentage of micropores results in lower acoustic velocities for a given sample porosity (Eberli et al., 2003; Ali et al., 2018). Samples C15-C18, have the highest porosities and lowest acoustic wave velocities. The high secondary porosity is induced mainly by fracturing and dissolution of some intragranular components (bioclasts) which are common in these matrix-supported wackstones (Table 1). Moreover, samples C15 to C21 possess similarly low acoustic velocities (ranging from 2833 to 3236 m/s for  $V_p$ , and from 1605 to 1928 m/s for  $V_s$ ) at moderate-high porosity ranges. Samples C19 and C21 have very similar  $V_p$  of 3093 and 3150 m/s but porosities of 0.27 and 0.23, respectively. In addition, samples C1, C6, and C13 have very similar velocities of 2557, 2580, and 2512 m/s, respectively. Yet, they have very

different porosities of 0.072, 0.16, and 0.17. These samples have a variety of pore types such as intergranular, intragranular, fracture, and dissolution pores (Table 1, and Fig. 5A). They have also very low permeability (Table 2) that is induced by the small grain size and the presence of micropores. There is no major difference in the acoustic velocities between pure calcite and dolomite (Anselmetti and Eberli, 1993, 2001). Therefore, we speculate that the observed variations in the acoustic velocities arise mainly from the rock texture and the diagenetic processes (Verwer et al., 2008). In the case of different velocities at the same porosity (Fig. 8B), the formation of a rigid structure at the time of early diagenesis gives a greater strength to the rocks than what is usual for their porosity. The cement type and the pore geometry may also contribute to the scatter in the  $\phi$ - $V_p$  plots (Dürrast and Siegesmund, 1999; Eberli et al., 2003). In general, the dense and less-porous marine carbonates have high  $V_p$  of 6260-6640 m/s, which resemble that of pure calcite (Mavko et al., 2009). Similar high  $V_p$  of 6060-6135 m/s and  $V_s$  ( $>3300$  m/s) have also been observed in our samples for very low-porosity ( $\phi \sim 0.02$ ) carbonate rocks (samples C2 and C3; Table 2), which are mainly grain-supported packstones (Table 1).

Results of  $\mu$ CT imaging on travertine samples examined by Soete et al. (2015) revealed that samples having similar porosities but varying velocities are significantly different. Samples of uniformly distributed pores give rise to a scattered wavefront and reduced velocities. On the other hand, samples with predominantly moldic pores have a stiff framework which envelops the sparite-depleted molds and give a limited wavefront scatter, and, therefore, higher velocities (Anselmetti and Eberli, 1993). Results of Saleh and Castagna (2004) revealed also that pores possessing high aspect ratios (e.g., vugs and molds) give a stronger support than intercrystalline and interparticle pores, hence making the rock much stiffer by reducing the pore compressibility at the same porosity. Therefore, at a given porosity, the seismic velocity decreases with the increase of the amount of micropores and

increases with the increase of the stiff moldic pores (e.g., Xu et al., 2009; Fournier et al., 2014). According to Brigaud et al. (2010), the widely-variable pore sizes and their shapes result in the encountered velocity fluctuations.

Samples C1-C4, C6-C10, and C13-C14 possess the highest incompressibility (Table 2). These samples are either packstone or wackstone and all have low/moderate porosity. Greater cementation may also contribute to the high incompressibility of some rocks in the present study. On the other hand, the wack-packstone and mud-wackstone microfacies as well as few wackstone rocks have lower incompressibilities and higher porosity. For example, sample C11 is a fractured, matrix-supported, mud-wackstone whose porosity and bulk modulus are 0.18 and  $1.85 \times 10^{10}$  Pa, respectively. The lowest incompressible samples are C15 to C21, which are highly porous, matrix-supported, wackstones or wack-packstones. In addition, dry limestone samples have generally higher Young's and shear moduli compared to those of the saturated samples in accordance with many previous studies (e.g., Vanorio et al., 2008).

Upon saturation, incompressibility increases at lower and intermediate porosities ( $\phi < \sim 0.25$ ). On the other hand, at porosities of larger than 0.30, there is a drop in the  $V_p$ , and accordingly the incompressibility of the rock decreases (Fig. 9A). In addition, the  $\phi$ - $V_p$  and  $\phi$ - $\kappa$  correlations are strong for the dry samples (Figs. 8A and 9A), but weak under saturation conditions in accordance with the results of Croizé et al. (2010). The better correlation under the dry conditions reflects basic similarities in pore geometry and matrix nature, which may revert after saturation. The observed high correlations between porosity and incompressibility and elasticity imply also that porosity is the main factor controlling such rock properties (Table 3). Indurated carbonates have high  $V_p/V_s$  ratios between 1.8 and 2.0 (Anselmetti and Eberli, 1993). However, our samples exhibit generally lower ratios, which vary from 1.6 to 1.83, and with an average of 1.73. Therefore, we speculate that cementation, rather than mechanical compaction, played a major role in the evolution of the physical properties of the

studied rocks. Previous researchers found weak correlations between the elastic moduli and porosity implying that other parameters related mainly to the rock pore system control the stiffness of carbonate rocks (Croizé et al., 2010).

### ***5.3. A possible diagenetic sequence***

The diagenetic potential of carbonates is controlled largely by the rock texture and the amount of metastable components (Schlanger and Douglas, 1974). Fine-grained, mud-supported, carbonate rocks have very low permeability; thus diagenetic alterations are very limited, resulting in low acoustic velocities (Awais et al., 2018).

Through the petrographic analysis and the results obtained from the petrophysical measurements, we propose a complete paragenetic sequence for the studied rocks (e.g., Awais et al. 2018). The initial environment was marine. Subsequent diagenesis represented by the mixed marine-meteoric, meteoric and burial diagenesis followed and affected the sediments (Fig. 11). Samples C1-C4 showed the mixed marine-meteoric to meteoric diagenesis which is evidenced by the existence of cementation, dissolution and dolomitization, while early marine diagenesis has been observed in samples C5-C10 and C13-C18 through the clear signals of micritization. Samples C11 and C12 exhibit different diagenesis during burial of the sediments where they were highly fractured.

## **6. Conclusions**

In this study, we examined the effects of porosity, pore types, and sediment characteristics on the petrophysical and acoustic properties of twenty-one carbonate rock samples collected from northern Lebanon. The petrographical and SEM analyses revealed that the studied rocks are either grain-supported packstone or matrix-supported wackstone, mudstone/wackstone, and wackstone/packstone with variable grain and porosity types.

Porosity and bulk density vary generally widely. The primary rock framework and diagenetic alterations contribute to the observed wide ranges of porosity (up to 32%). The rock textures and the high percentage of microporosity in matrix-supported rocks explain the observed low permeability. The acoustic wave velocities vary also widely and are inversely correlated with porosity. Some samples exhibit similar velocities at different porosities. The acoustic velocities in porous samples are reduced by more than 50% of the velocity in the compact, less-porous, rocks. The inverse correlation between velocity and porosity points to the strong impact of the later on acoustic velocity. The soft, porous, limestones are more compressible and have lower elastic moduli, and thus lower velocities. On the other hand, stiff, less-porous, rocks have higher elastic moduli and higher acoustic velocities. The  $V_p/V_s$  ratio varies from 1.60 to 1.83 (average 1.73), which is low compared to values characteristic for marine carbonates and can be interpreted by the cementation of less mechanically-compacted rocks. To sum up, the acoustic properties of carbonate rocks are controlled by their depositional conditions and the subsequent diagenetic processes which modify their pore types and sizes.

Different pore shapes have different compressibilities and accordingly, different acoustic velocities. Upon saturation, the Young's modulus and rigidity decreased compared to their equivalent values of the dry rocks. Porosity value is critical in the behavior of  $V_p$  under saturation; it is reduced if the porosity is greater than about 0.15. Cementation by fine components plays a major role on velocity at higher porosities causing a positive departure from the best-fit line. On the other hand, stiffening by cementation of the rock frame at lower porosities is limited because of the already compact nature and the high packing of the low-porosity rocks.

Acoustic velocities and the elastic moduli are positively correlated to bulk densities. The acoustic impedance of the studied samples varies widely due to the wide variations in seismic

velocity and bulk density. It exhibits a strong inverse correlation with porosity, therefore, not all reflectors encountered in carbonate rocks are the result of different mineralogy or even lithology. Rather, they may be induced by complex pore geometry and different types of pores encountered. The obtained results of porosity, permeability, density, acoustic velocities, and the calculated elastic moduli of the studied rocks are important in seismic exploration and well log studies in equivalent subsurface marine carbonate reservoirs.

### **Acknowledgments**

SEM images were taken in the Central Research Science Laboratory/American University of Beirut and the Digital photographs have been taken in the Laboratory Center at the Yarmouk University.

### **References**

- Adam, L., Batzle, M., Brevik, I., 2006. Gassmann's fluid substitution and shear modulus variability in carbonates at laboratory seismic and ultrasonic frequencies. *Geophysics*, 71 (6), F173–F183.
- Akbar, M., Vissarpragada, B., Alghamdi, A. H., Allen, D., Herron, M., Carnegie, A., Dutta, D., Olesen, J.-R., Chourasiya, R. D., Logan, D., Steif, D., Netherwood, R., Russell, S. D., Saxena, K. 2001. A snapshot of carbonate reservoir evaluation. *Oilfield Review*, 12, 20-41.
- Ali, A., Wagneich, M., Strasser, M., 2018. Depositional constraints and diagenetic pathways controlling petrophysics of Middle Miocene shallow-water carbonate reservoirs (Leitha limestones), Central Paratethys, Austria-Hungary. *Marine and Petroleum Geology*, 91, 586-598. <https://doi.org/10.1016/j.marpetgeo.2018.01.031>
- Alqudah, M., Monzer, A., Sanjuan, J.; Salah, M. K., Alhejoj, I. K., 2019. Calcareous nanofossil, nummulite and ostracod assemblages from Paleocene to Miocene successions in the Bekaa Valley (Lebanon) and its paleogeographic implications. *J. Afr. Earth Sci.*, 151, 82-94. <https://doi.org/10.1016/j.jafrearsci.2018.12.001>

- Amyx, J. W., Bass, D. M., Whiting, R. L., 1960. Petroleum reservoir engineering - physical properties, McGraw-Hill New York, USA.
- Anselmetti, F. S., Eberli, G. P., 1993. Controls on sonic velocity in carbonates. *Pure and Applied Geophysics*, 141 (2–4), 287–323.
- Anselmetti, F. S., Eberli, G. P., 2001. Sonic velocity in carbonates - a combined product of depositional lithology and diagenetic alterations. In: Ginsburg, R. (Ed.), *Subsurface Geology of a Prograding Carbonate Platform Margin, Great Bahama Bank: Results of the Bahamas Drilling Project*. SEPM Special Publication, 70, 193–216.
- Awais, M., Hanif, M., Khan, M. Y., Jan, I. U., Ishaq, M., 2018. Relating petrophysical parameters to petrographic interpretations in carbonates of the Chorgali Formation, Potwar Plateau, Pakistan. *Carbonates and Evaporites*, <https://doi.org/10.1007/s13146-017-0414-x>
- Beydoun, Z. R., 1988. *The Middle East: Regional Geology and Petroleum Resources*. Scientific Press Limited, Beaconsfield, U.K., 292 p.
- Birch, F., 1960. The velocity of compressional waves in rocks to 10 kilobars, part 1. *J. Geophys. Res.*, 65 (4), 1083–1102.
- Brigaud, B., Vincent, B., Durllet, C., Deconinck, J.-F., Blanc, P., Trouiller, A., 2010. Acoustic properties of ancient shallow-marine carbonates: effects of depositional environments and diagenetic processes (Middle Jurassic, Paris Basin, France). *J. Sediment. Res.*, 80 (9), 791-807.
- Brown, A., 1997. Porosity variation in carbonates as a function of depth: mississippian madison group, williston basin. In: Kupecz, J., Gluyas, J., Bloch, S. (Eds.), *Reservoir Quality Prediction in Sandstones and Carbonates: AAPG Memoir*, 69, 29–46.
- Buckley, J. P., Elders, C., Mann, J., 2013. Carbonate Buildups in the Santos Basin, offshore Brazil. Programme and abstract volume: microbial carbonates in space and Time: implications for global exploration and production. *Geol. Soc. Lond.*, 37-39.
- Burnett, J. 1998. Upper Cretaceous. In P. Bown (Ed.), *calcareous nannofossils biostratigraphy*. Chapman and Hall, London, p. 132-199.
- Cassar, J., 2016. The Historic and Archaeological Heritage: Pollution and Non-Urban Sites. In: *Urban Pollution and Changes to Materials and Building Surfaces*, 255-290, P. Brimblecombe (ed). Imperial College Press.

- Cerepi, A., Burlot, R., Humbert, L. 1999. Effects of carbonate rock-fabrics on the petrophysical properties. In: Transferts dans les systèmes sédimentaires : de l'échelle du pore à celle du bassin. Réunion spécialisée SGF-TRABAS/CNRS, Paris 27- 28 septembre 1999. Résumés. Strasbourg : Institut de Géologie – Université Louis-Pasteur, 1999. pp. 45-48. (Sciences Géologiques. Mémoire, 99).
- Cerepi, A., Barde, J., Labat, N. 2003. High-resolution characterisation and integrated study of a reservoir formation: the danian carbonate platform in the Aquitaine Basin (France). *Marine and Petroleum Geology*, 20, 1161-1183.
- Chuhan, F. A., Kjeldstad, A., Bjørlykke, K., Høeg, K., 2003. Experimental compression of loose sands; relevance to porosity reduction during burial in sedimentary basins. *Canadian Geotechnical Journal-Revue Canadienne de Geotechnique* 40 (5), 995–1011.
- Croizé, D., Ehrenberg, S. N., Bjørlykke, K., Renard, F., Jahren, J., 2010. Petrophysical properties of bioclastic platform carbonates: implications for porosity controls during burial. *Marine and Petroleum Geology*, 27, 1765-1774.  
doi:10.1016/j.marpetgeo.2009.11.008
- de Ruiter, R. S. C., Lovelock, P. E. R., Nabulsi, N., 1995. The Euphrates Graben of Eastern Syria: A New Petroleum Province in the Northern Middle East. In M.I. Al-Husseini (Ed.), *Middle East Petroleum Geosciences, GEO'94*. Gulf PetroLink, Bahrain, 1, 357-368.
- Dewit, J., Huysmans, M., Muchez, P., Hunt, D. W., Thurmond, J. B., Verges, J., Saura, E., Fernandez, N., Romaine, I., Esestime, P., Swennen, R., 2012. Reservoir characteristics of fault-controlled hydrothermal dolomite bodies: Ramales Platform case study. *Geol. Soc. Lond. Special Publications*, 370 (1), 83-109.
- Dunham, R. J., 1962. Classification of carbonate rocks according to their depositional texture. In W.E. Ham (Ed.), *Classification of Carbonate Rocks - A Symposium*. Tulsa, OK, American Association of Petroleum Geologists Memoir 1, 108-121.
- Dürrast, H., Siegesmund, S., 1999. Correlation between rock fabrics and physical properties of carbonate reservoir rocks. *Int. J. Earth Sci.*, 88 (3), 392–408.
- Eberli, G. P., Baechle, G. T., Anselmetti, F. S., Incze, M. L., 2003. Factors controlling elastic properties in carbonate sediments and rocks. *The Leading Edge*, 22 (7), 654–660.

- Ehrenberg, S. N., Eberli, G. P., Keramati, M., Moallemi, S. A., 2006. Porosity–permeability relationships in interlayered limestone–dolostone reservoirs. *AAPG Bulletin*, 90 (1), 91–114.
- Ehrenberg, S. N., Nadeau, P. H., 2005. Sandstone vs. carbonate petroleum reservoirs; a global perspective on porosity - depth and porosity – permeability relationships. *AAPG Bulletin*, 89 (4), 435–445.
- El Sayed, N. A., Abuseda, H., Kassab, M. A., 2015. Acoustic wave velocity behavior for some Jurassic carbonate samples, north Sinai, Egypt. *J. Afr. Earth Sci.*, 111, 14-25.  
<http://dx.doi.org/10.1016/j.jafrearsci.2015.07.016>
- Flügel, E., 1982. *Microfacies Analysis of Limestone*. Springer-Verlag, Berlin, 663 p.
- Fournier, F., Leonide, P., Kleipool, L., Toullec, R., Reijmer, J. J. G., Borgomano, J., Klootwijk, T., Van Der Molen, J., 2014. Pore space evolution and elastic properties of platform carbonates (Urgonian limestone, Barremian–Aptian, SE France). *Sediment. Geol.*, 308, 1-17.
- Freire-Lista, D. M., Fort, R., 2017. Historical quarries, decay and petrophysical properties of carbonate stones used in the historical center of Madrid (Spain). *AIMS Geosciences*, 3 (2): 284-303. DOI: 10.3934/geosci.2017.2.284
- Freire-Lista, D. M., Fort, R., Varas-Muriel, M. J., 2016. Thermal stress-induced microcracking in building granite. *Engineering Geology*, 206. DOI: 10.1016/j.enggeo.2016.03.005
- Friedman, G. M., 1964. Early diagenesis and lithification in carbonate sediments. *J. Sediment. Res.*, 34 (4), 777–813.
- Hamilton, E. L., 1976. Variations of density and porosity with depth in deep-sea sediments. *J. Sediment. Pet.*, 46 (2), 280–300.
- Harmon, R. S., Wicks, C. M., 2006. Perspectives on karst geomorphology, hydrology, and geochemistry - A tribute Volume to Derek C. Ford and William B. White. *Geological Society of America*, vol. 404. DOI: <https://doi.org/10.1130/SPE404>
- Jin, X., Dou, Q., Hou, J., Huang, Q., Sun, Y., Jiang, Y., Li, T., Sun, P., Sullivan, C., Adersokan, H., Zhang, Z., 2017. Rock-physics-model-based pore type characterization and its implication for porosity and permeability qualification in a deeply-buried

carbonate reservoir, Changxing formation, Lower Permian, Sichuan Basin, China. *J. Petrol. Sci. Eng.*, 153, 223-233.

<http://dx.doi.org/10.1016/j.petrol.2017.02.003>

Kearey, P., Brooks, M., Hill, I., 2002. *An Introduction to Geophysical Exploration*. Blackwell Publishing, 262 pp.

Kennedy, M. C. 2002. Solutions to some problems in the analysis of well logs in carbonate rocks. In: Lovell, M. & Parkinson, N. (eds.) *Geological applications of wireline logs*. AAPG, London United Kingdom, 13, 61-73.

Kerans, C., 1988. Karst-controlled reservoir heterogeneity in Ellenburger Group carbonates of west Texas: Reply, *AAPG Bulletin*, 72, 1160-1183.

Klinkenberg, L. J., 1941. The permeability of porous media to liquids and gases. *Am. Pet. Inst., Drilling and Productions Practices*, 200–213.

Lapponi, F., Casini, G., Sharp, I., Blendinger, W., Fernandez, N., Romaine, I., Hunt, D., 2011. From outcrop to 3D modelling: a case study of a dolomitized carbonate reservoir, Zagros Mountains. *Iran. Pet. Geosci.*, 17 (3), 283-307.

Li, H., Zhang, J., 2011. Elastic moduli of dry rocks containing spheroidal pores based on differential effective medium theory. *J. Appl. Geophys.*, 75 (4), 671–678.

<http://dx.doi.org/10.1016/j.jappgeo.2011.09.012>

Litak, R. K., Barazangi, M., Brew, G., Sawaf, T., Al-Imam, A., Al-Youssef, W., 1998. Structure and Evolution of the Petroliferous Euphrates Graben System, Southeast Syria. *AAPG Bulletin*, 82, 1173-1190.

Loucks, R. G., 1999. Paleocave carbonate reservoirs: origins, burial-depth modifications, spatial complexity, and reservoir implications. *AAPG Bulletin*, 83, 1795-1834.

Loucks, R. G., 2001. Modern analogs for paleocave-sediment fills and their importance in identifying paleocave reservoirs. *Transactions, Gulf Coast Association of Geological Societies*, 195-206.

Loucks, R. G., Handford, C. R., 1992. Origin and recognition of fractures, breccias, and sediment fills in paleocave reservoir networks. *Publication - Society of Economic Paleontologists and Mineralogists, Permian Basin Chapter*, 92-33, 31-44.

- Loucks, R. G., Mescher, P., 2001. Published, Paleocave facies classification and associated pore types, in Proceedings American Association of Petroleum Geologists, Southwest Section, Annual Meeting, Dallas, Texas, p. 18.
- Lucia, F. J., 1995. Rock-Fabric/Petrophysical Classification of Carbonate Pore Space for Reservoir Characterisation. AAPG Bulletin, 79, 1275-1300.
- Lucia, F. J., 1999. Characterization of petrophysical flow units in carbonate reservoirs: Discussion. AAPG Bulletin, 83, 1161-1163.
- Lucia, F. J. 2000. Dolomitisation: A Porosity-Destructive Process. 2000-2001 AAPG distinguished lecturers; abstracts AAPG Bulletin, 84, 1879.
- Lucia, F. J., 2007. Carbonate reservoir characterization. 2nd edition, Springer-Verlag Berlin Heidelberg.
- Mavko, G., Mukerji, T., Dvorkin, J., 2009. The Rock Physics Handbook, 2<sup>nd</sup> Ed. Cambridge.
- Mazzullo, S., Chilingarian, G., 1996. Hydrocarbon reservoirs in karsted carbonate rocks. Developments in Petroleum Science, 44, 797-865.
- Nader, F. H., 2014. The geology of Lebanon. Scientific Press Ltd, United Kingdom, p. 108.
- Neto, I. A. L., Misságia, R. M., Ceia, M. A., Archilha, N. L., Oliveira, L. C., 2014. Carbonate pore system evaluation using the velocity-porosity-pressure relationship, digital image analysis, and differential effective medium theory. J. Appl. Geophys., 110, 23-33. <http://dx.doi.org/10.1016/j.jappgeo.2014.08.013>
- Nurmi, R., Standen, E., 1997. Carbonates, the inside story. Middle East Well Eval. Rev., 18, 28-41.
- Russell, B. H., Smith, T., 2007. The relationship between dry rock bulk modulus and porosity—an empirical study. CREWES Res. Rep., 19,1–14.
- Salah, M. K., Alqudah, M., El-Al, A.A., Barnes, C., 2018. Effects of porosity and composition on seismic wave velocities and elastic moduli of Lower Cretaceous rocks, central Lebanon. Acta Geophysica, 66(5), 867-894. <https://doi.org/10.1007/s11600-018-0187-1>
- Salah, M. K., Alqudah, M., Monzer, A. J., David, Ch., 2020. Petrophysical and acoustic characteristics of Jurassic and Cretaceous rocks from Central Lebanon. Carbonates and Evaporites, 35:12. <https://doi.org/10.1007/s13146-019-00536-w>

- Saleh, A. A., Castagna, J. P., 2004. Revisiting the Wyllie time average equation in the case of near spherical pores. *Geophysics*, 69, 45–55. <http://dx.doi.org/10.1190/1.1649374>
- Schlanger, S. O., Douglas, R. G., 1974. The pelagic ooze-chalk-limestone transition and its implications for marine stratigraphy. In: Hsu KJ, Jenkyns HC (eds) *Pelagic sediments on land and under the sea*. Internat. Assoc. Sed. Spec. Publ., 1, 117–148.
- Schmoker, J. W., 1984. Empirical relation between carbonate porosity and thermal maturity - an approach to regional porosity prediction. *AAPG Bulletin*, 68 (11), 1697–1703.
- Scholle, P. A., Halley, R. B., 1985. Burial diagenesis; out of sight, out of mind! In: Schneidermann, N., Harris Paul, M. (Eds.), *Carbonate Cements Special Publication-Society of Economic Paleontologists and Mineralogists. SEPM (Society for Sedimentary Geology)*, 36. United States, Tulsa, OK, 309–334.
- Soete, J., Kleipool, L. M., Claes, H., Hamaekers, H., Kele, S., Özkul, M., Foubert, A., Reijmer, J. J. G., Swennen, R., 2015. Acoustic properties in travertines and their relation to porosity and pore types. *Marine and Petroleum Geology*, 59, 320-335. <http://dx.doi.org/10.1016/j.marpetgeo.2014.09.004>
- Sun, Y. F., Berteussen, K., Vega, S., Eberli, G. P., Baechle, G. T., Weger, R. J., Massaferro, J. L., Bracco Gartner, G. L., Wagner, P. D., 2006. Effects of pore structure on 4D seismic signals in carbonate reservoirs. *SEG Technical Program Expanded Abstracts*, 3260–3264. <http://dx.doi.org/10.1190/1.2370208>
- Vanorio, T., Scotellaro, C., Mavko, G., 2008. The effect of chemical and physical processes on the acoustic properties of carbonate rocks. *The Leading Edge*, 27 (8), 1040–1048.
- Varol, O., 1991. New Cretaceous and Tertiary calcareous nannofossils. - *N. Jb. Geol. Palaont., Abh.*, 1 82: 2 1 1 -237; Stuttgart.
- Verwer, K., Braaksma, H., Kenter, J. A. M., 2008. Acoustic properties of carbonates: effects of rock texture and implications for fluid substitution. *Geophys.*, 73 (2), B51–B65.
- Walley, C. D., 1983. A revision of the Lower Cretaceous stratigraphy of Lebanon. *Geologische Rundschau*, 72(1), 377-388.
- Walley, C. D., 1997. The lithostratigraphy of Lebanon: a review. *Lebanese Science Bulletin*, 10:1.
- Wang, Z., Hirsche, W. K., Sedgwick, G., 1991. Seismic velocities in carbonate rocks. *Can. Pet. Tech.*, 30, 112-122.

- Wilson, J. L., 1975. Carbonate facies in geologic history. Springer-Verlag, New York, 471 p.
- Xu, S., Payne, M., Exxonmobil, 2009. modeling elastic properties in carbonate rocks. Lead. Edge, 66-74.
- Yu, C., Ji, S., Li, Q., 2016. Effects of porosity on seismic velocities, elastic moduli and Poisson's ratios of solid materials and rocks. J. Rock Mech. Geotech. Eng., 8, 35–49. <https://doi.org/10.1016/j.jrmge.2015.07.004>
- Zolotukhin, A. B., Ursin, J.-R., 2000. Introduction to petroleum reservoir engineering, Kristiansand, Høyskoleforlaget AS - Norwegian Academic Press, 402 p.

Calcareous nannofossil taxonomic list:

- Amphizygus* Bukry 1969  
*A. brooksii* Bukry 1969  
*Broinsonia* Bukry 1969  
*B. parca* (Stradner 1963) Bukry 1969  
*Discorhabdus* Noël 1965  
*D. ignotus* (Górka 1957) Perch-Nielsen 1968  
*Eiffellithus* Reinhardt 1965  
*Eiffellithus eximius* (Stover, 1966) Perch-Nielsen, 1968  
*Gartnerago* Bukry 1969  
*G. segmentatum* (Stover 1966) Thierstein 1974  
*Lapideacassis* Black 1971  
*Lapideacassis mariae*

*Prediscosphaera* Vekshina 1959  
*P. cretacea* (Arkhangelsky 1912) Gartner 1968  
*Rotelapillus* Noël, 1973  
*Rotelapillus laffitei*, syn. *Rotelapillus crenulatus* (Stover, 1966) Perch-Nielsen, 1984  
*Tranolithus* Stover 1966  
*T. minimus* (Bukry 1969) Perch-Nielsen 1984  
*T. orionatus* (Reinhardt 1966) Perch-Nielsen 1968 = *T. phacelosus*  
*Watznaueria* Reinhardt 1964  
*W. barnesiae* (Black 1959) Perch-Nielsen 1968  
*Zeugrhabdotus* Reinhardt 1965

## Figure Captions

**Fig. 1.** Geological map showing the ages and major structures of the Lebanese rocks. the inset shows the locations of the sampled sections in Batroun and Chekka areas in north central Lebanon.

**Fig. 2.** Panoramic view of Batroun (1), and Chekka (2) outcrops along with the locations of the drilled core samples.

**Fig. 3.** Two columnar sections representing the Cenomanian-Turonian succession in Batroun and the Campanian succession in Chekka.

Fig. 4. The Klinkenberg correction plot for the accurate estimation of rock permeability. Extrapolation of the straight lines intersects the vertical axis in a value which corresponds to the liquid permeability. Three samples: C8, C15, and C21 are shown on the plot with corresponding permeabilities of 0.075, 0.06, and 0.067 mD, respectively.

**Fig. 5.** The different types of microfacies detected in the studied samples. Note the heterogeneities in the pore sizes and shapes (see text for more details). Interlocking crystal grains are clear in A; while rhombic dolomite is clear in B. Calcitic grains within dolomitic matrix are observed in C and D; bioclasts are represented in the samples by bone fragments (E), spines (F), gastropods (G and Q), ostracods (H and O), echinoids (I), and both benthonic and planktonic foraminifera (J and P). The moderate to poor preservation of fossils is shown in R; different porosity types are observed in K, L, M, N, S, and T (refer to the text for more details).

**Fig. 6.** Different calcareous nannofossil assemblages detected in the studied samples (refer to the text for more details).

**Fig. 7.** Cross plots between different petrophysical parameters: porosity vs. bulk density (A); porosity vs. permeability (B); grain density vs. porosity (C); and grain density vs. bulk density (D).

**Fig. 8.** Cross plots between different petrophysical and acoustic parameters: porosity vs.  $V_p$  (A); porosity vs.  $V_s$  (B); porosity vs. Poisson's ratio (C); and porosity vs. acoustic impedance (D), for the dry (blue rhombs) and the water-saturated (red squares) cores.

**Fig. 9.** Cross plots between porosity and different elastic moduli: porosity vs. bulk modulus (A); porosity vs. shear modulus (B); and porosity vs. Young's modulus (C), for the dry (blue rhombs) and the water-saturated (red squares) cores.

**Fig. 10.** Cross plots between density and acoustic velocities: bulk density vs. acoustic velocities (A); and grain density vs. acoustic velocities (B). The blue rhombs and the red squares denote  $V_p$ , and  $V_s$ , respectively.

**Fig. 11.** The paragenetic sequence of the different diagenetic processes observed in the studied samples.

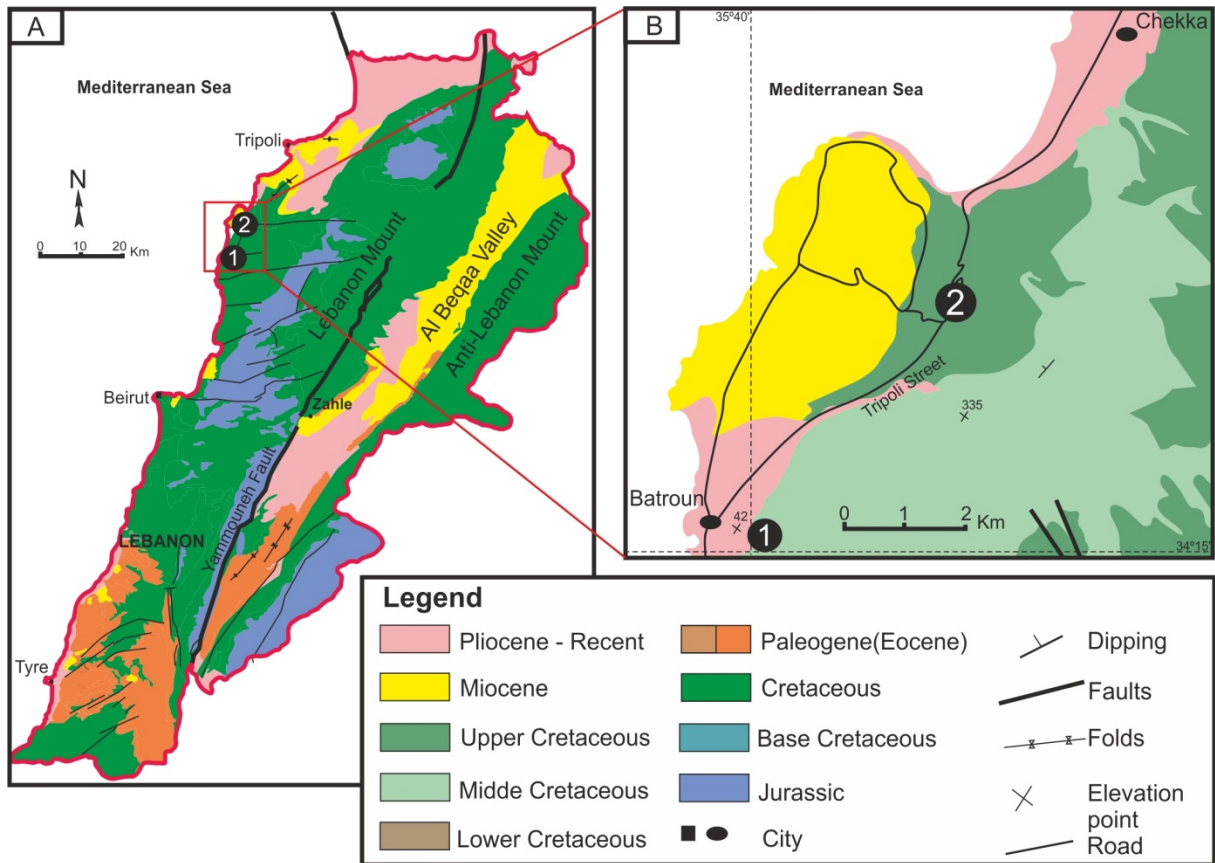


**Figure 1**



- ① Batroun section
- ② Chekka section
- Core plug sample

Figure 2

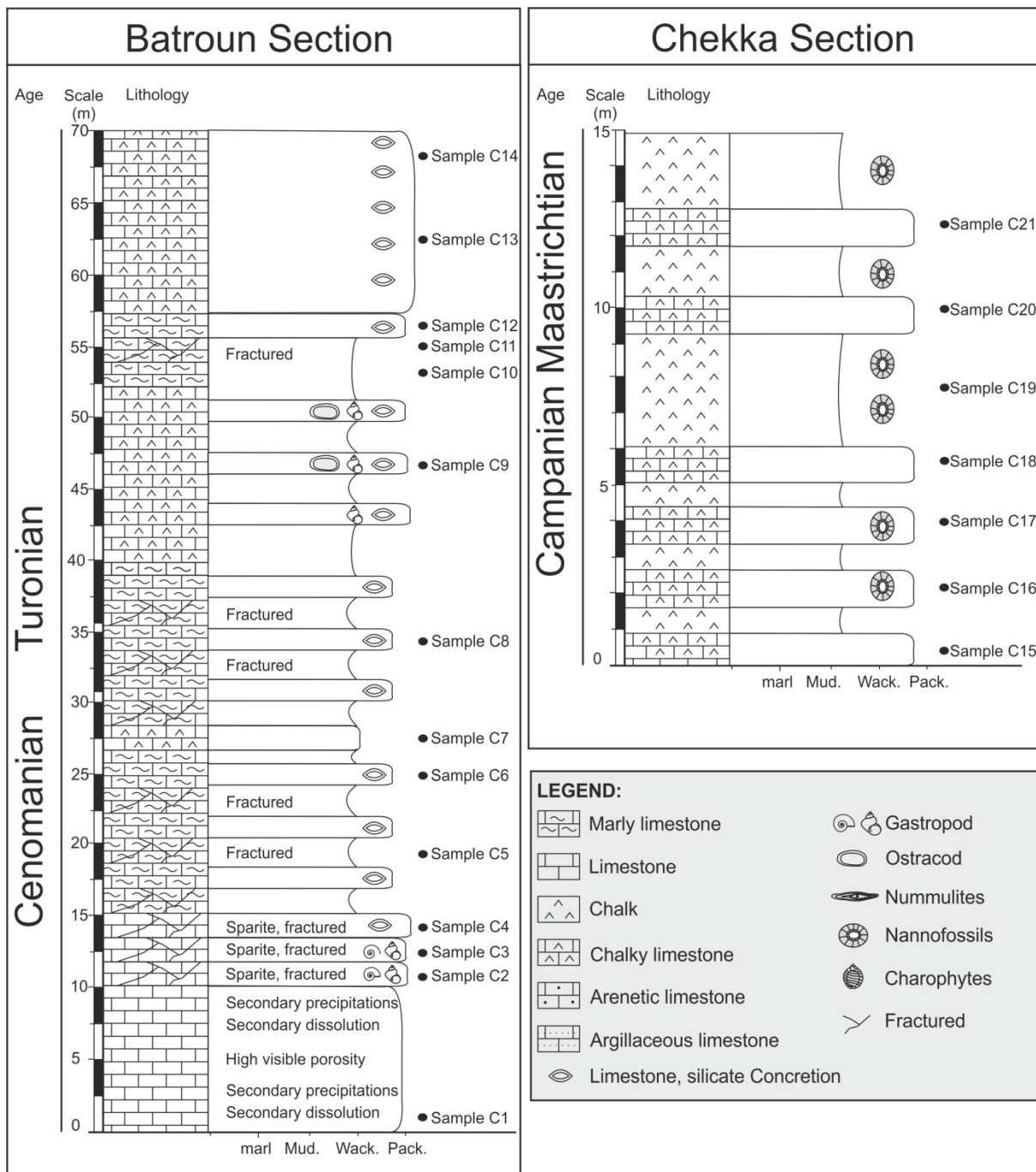


Figure 3

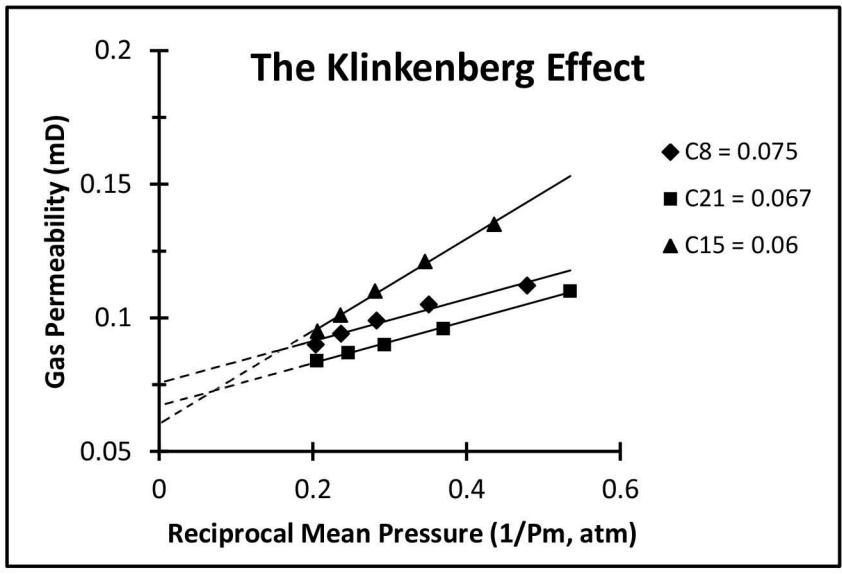
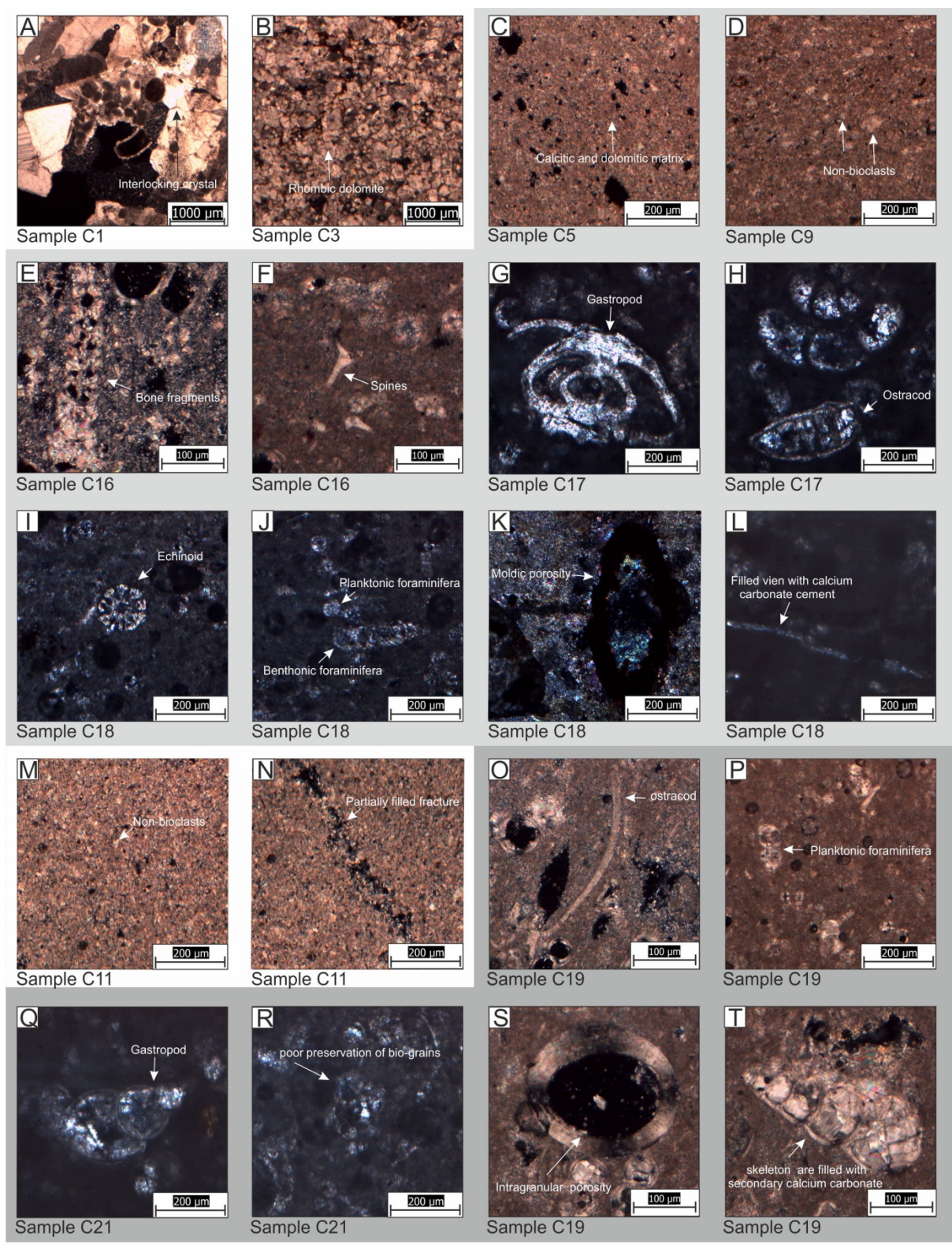
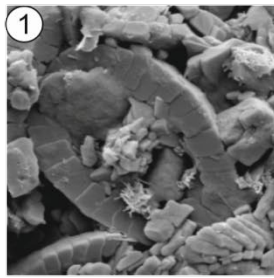


Figure 4

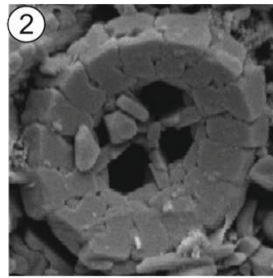


**Figure 5**

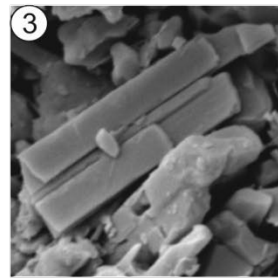
1 Micro  
▬



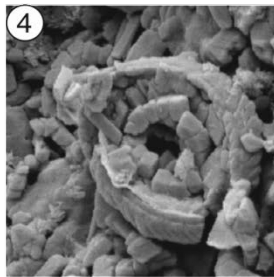
*Amphizygus brooksii*, C19



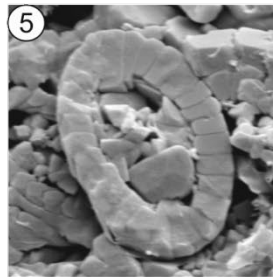
*Predicosphaera cretacea*, C19



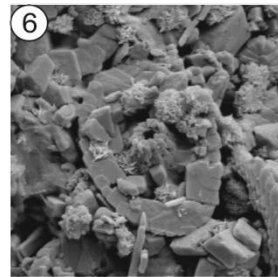
*Lapideacassis mariae*, C19



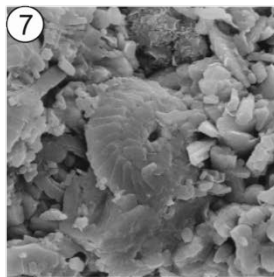
*Tranolithus minimus*, C19



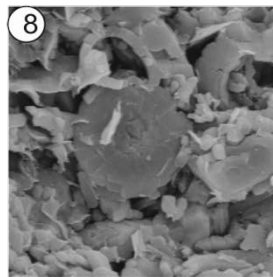
*Tranolithus orionatus*, C20



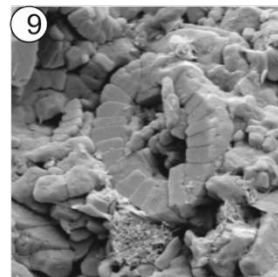
*Eiffelithus eximius*, C20



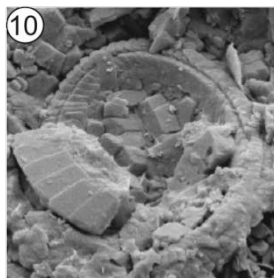
*Watznaueria barnesiae*, C20



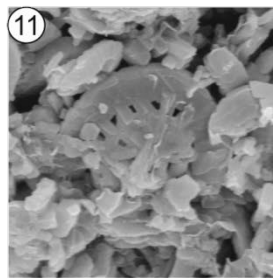
*Discorhabdus ignotus*, C20



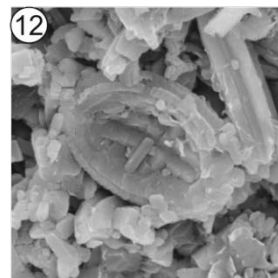
*Zeugrhabdotus* sp., C20



*Rotelapillus laffittei*, C21



*Broinsonia parca*, C21



*Gartnerago segmentatum*, C21

**Figure 6**

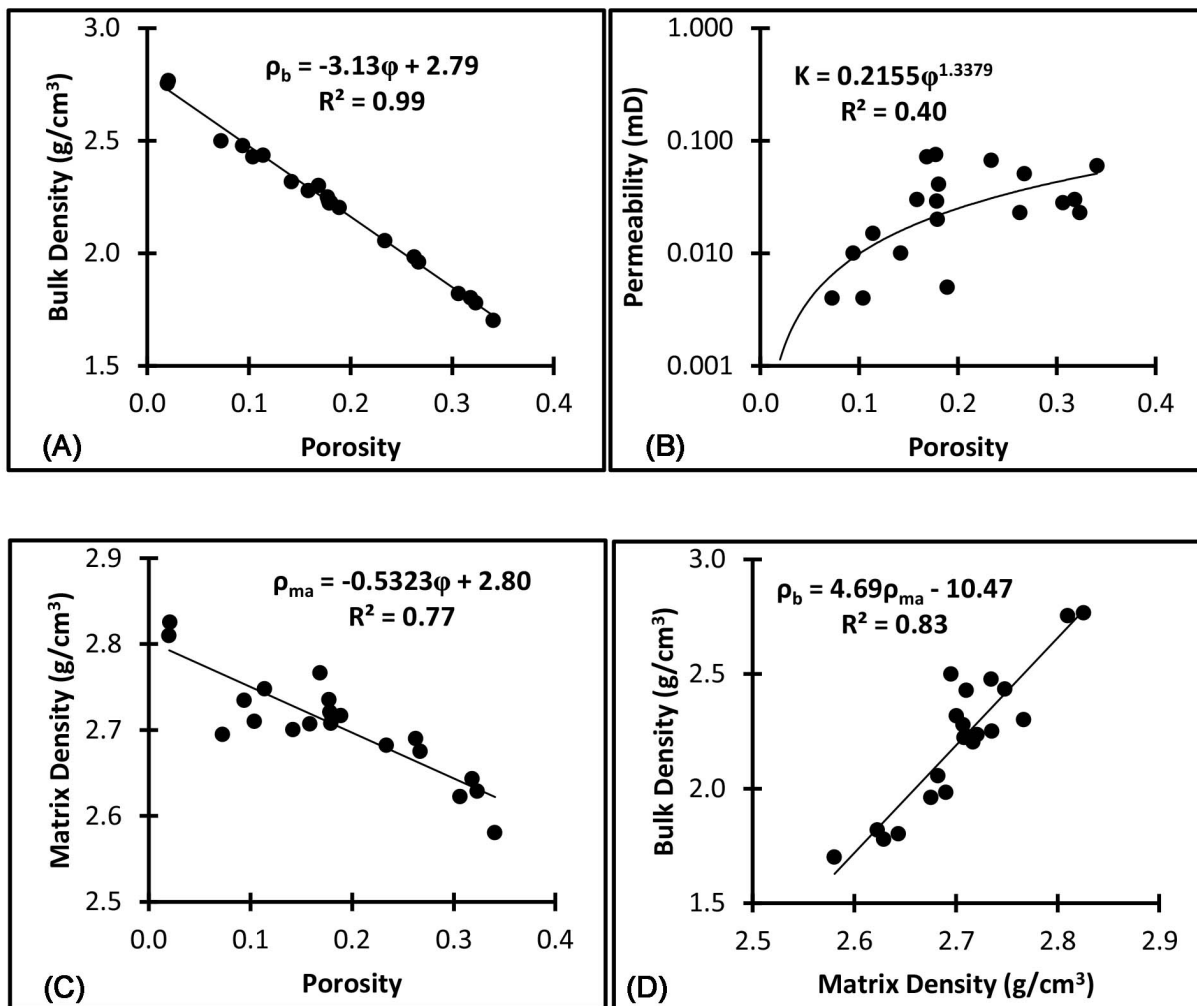


Figure 7

Figure 7

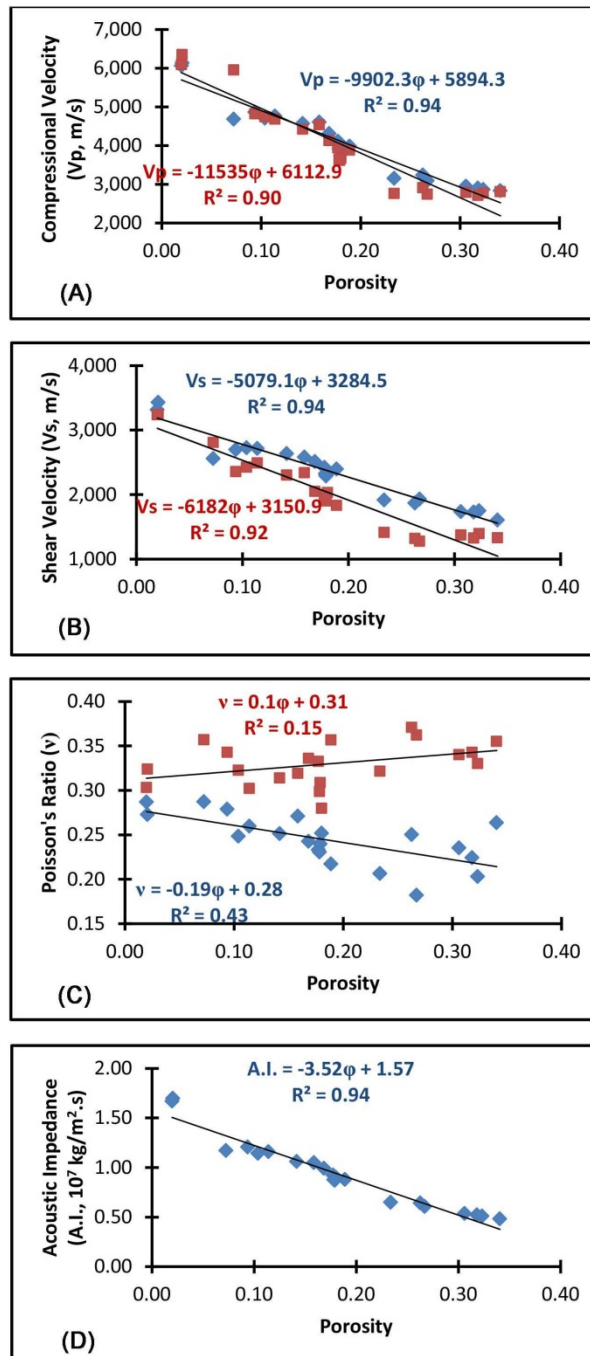


Figure 8

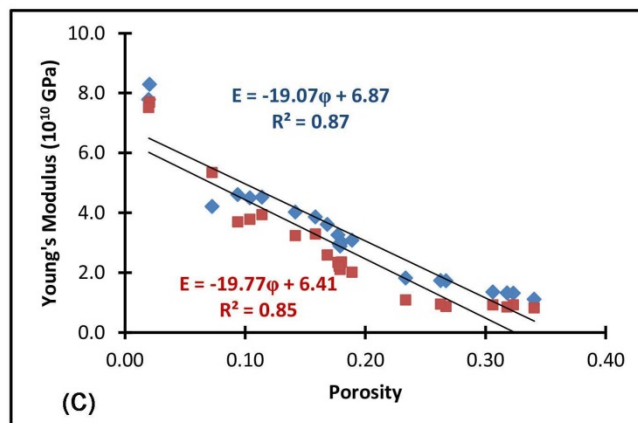
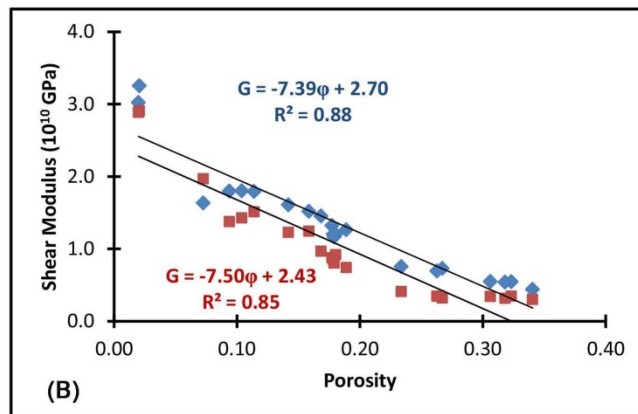
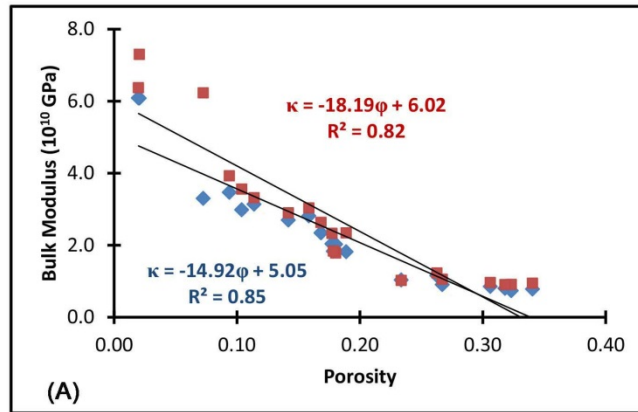


Figure 9

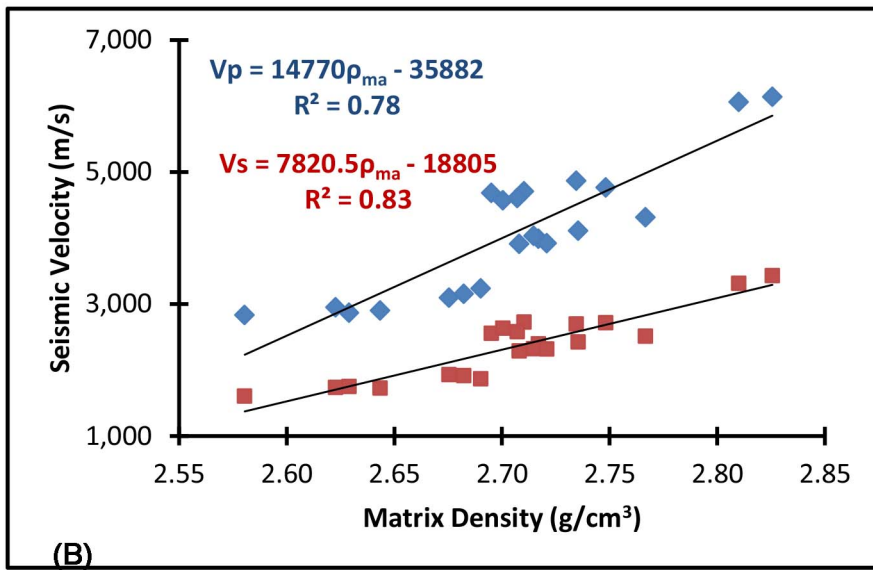
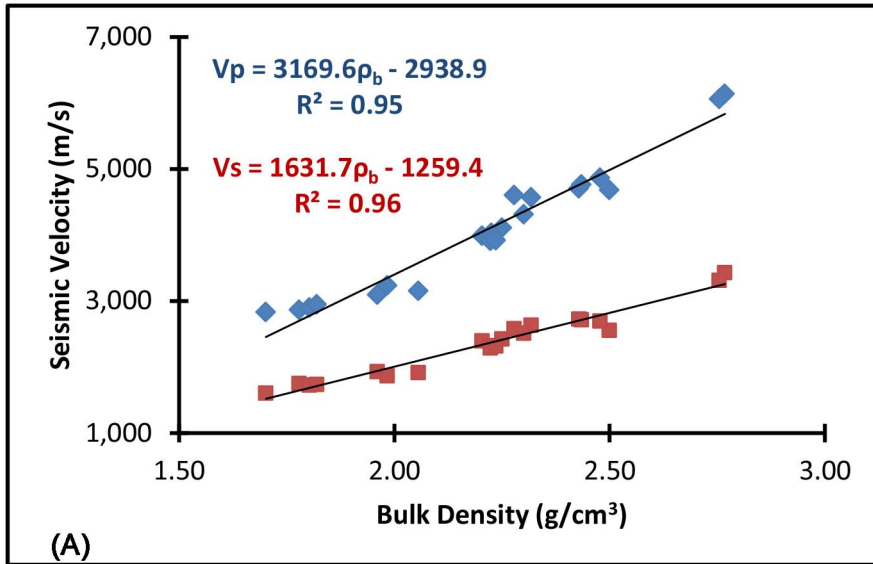


Figure 10

Samples	Diagenesis Processes	Diagenetic Environment			
		Marine	Mixed-marine-meteoritic	Meteoric	Burial
<div style="display: flex; flex-direction: column; align-items: center;"> <div style="border: 1px solid black; padding: 2px; margin-bottom: 10px;">C1 - C4</div> <div style="display: flex; gap: 20px;"> <div style="border: 1px solid black; padding: 2px;">C5 - C6</div> <div style="border: 1px solid black; padding: 2px;">C6- C10, C13-18</div> </div> <div style="border: 1px solid black; padding: 2px; margin-top: 10px;">C11 - C12</div> </div>	Micritization	↔			
	Dolomitization		↔		
	Dissolution			↔	
	Cementation			↔	
	Fracturing				↔

Figure 11

**Table 1:** The summary of the petrographical investigations of the thin sections prepared from the collected samples.

Sample No.	Rock Name	Grain Ratio		Porosity	Matrix	Cement	Crystal shapes	Grain Size and Packing
		Bioclast	Non-Bioclast					
C1-C2	Packstone	0%	Calcitic-phosphatic	Dissolution: etching and enlargement	5%	Calcitic sparite	Interlocking calcite crystals	Grain-supported
C3-C4	Packstone	0%	20% calcite 80% dolomite	Intergranular caused by dolomitization	Iron oxide and calcite	Sparite is rare	Well-sorted crystals	Grain-supported
C5-C7	Wackstone	10%, ostracods weathered	30% calcitic overgrowth	Intragranular, intergranular, and fractures	50%, calcitic and dolomitic	Calcitic fill in the veins	Irregular crystal shapes	Matrix-supported
C8	Wackstone	10%, Bone fragment, spines, weathered ostracods	5% reworked calcite crystals	Intragranular caused by dissolution, intergranular	Calcitic micrite	Calcitic fill in the veins	Arranged	Matrix-supported
C9-C10	Wackstone	5%, Baculites, planktonic foraminifera, ostracods	15% reworked calcite crystals	Intragranular	80% calcitic micrite	No sparite	Compacted	Matrix-supported
C11-C12	Mudstone-Wackstone	2%, Ostracods	5% calcitic crystals	Fractures filled by calcite	93% calcitic micrite	Calcitic fill in the veins	--	Matrix-supported
C13-C14	Wackstone	10%, Bone fragment, planktonic and benthonic foraminifera, gastropods	10% calcite lithoclast	Intragranular, intergranular, and fractures	70% calcitic micrite		--	Matrix-supported
C15-C18	Wackstone	30%, Planktonic and benthonic foraminifera	5% calcite, rare	Intragranular, and fractures	Calcitic micrite	Calcitic fill in the veins	--	Matrix-supported
C19-C21	Wackstone-Packstone	30%, Well-preserved planktonic and benthonic foraminifera	5% calcite, rare	Intragranular	65% calcitic micrite	--	--	Matrix-supported

**Table 2.** Measured and calculated petrophysical and elastic parameters of the studied core samples.

S. No.	$\phi$	$\rho_b$	$\rho_{ma}$	$K, mD$	Vp	Vs	A.I	$\nu$	E	$\kappa$	$\mu$	Vp sat	Vs sat	$\nu$ sat	E sat	$\kappa$ sat	$\mu$ sat
C1	0.072	2.50	2.70	0.004	4681	2557	1.17	0.29	4.21	3.30	1.63	5950	2806	0.36	5.34	6.22	1.97
C2	0.021	2.77	2.83	-	6135	3429	1.70	0.27	8.28	6.08	3.25	6353	3241	0.32	7.70	7.29	2.91
C3	0.020	2.75	2.81	-	6061	3313	1.67	0.29	7.78	6.09	3.02	6090	3237	0.30	7.52	6.37	2.89
C4	0.104	2.43	2.71	0.004	4707	2723	1.14	0.25	4.50	2.98	1.80	4741	2426	0.32	3.78	3.55	1.43
C5	0.189	2.20	2.72	0.005	3986	2395	0.88	0.22	3.08	1.82	1.26	3884	1833	0.36	2.01	2.34	0.74
C6	0.159	2.28	2.71	0.030	4605	2580	1.05	0.27	3.86	2.81	1.52	4538	2338	0.32	3.28	3.03	1.24
C7	0.094	2.48	2.73	0.010	4866	2695	1.21	0.28	4.60	3.47	1.80	4820	2357	0.34	3.70	3.92	1.38
C8	0.177	2.25	2.74	0.075	4108	2423	0.92	0.23	3.26	2.04	1.32	3940	1974	0.33	2.34	2.32	0.88
C9	0.180	2.23	2.71	0.041	4033	2322	0.90	0.25	3.01	2.02	1.20	3675	2031	0.28	2.35	1.78	0.92
C10	0.114	2.43	2.75	0.015	4763	2713	1.16	0.26	4.52	3.13	1.79	4680	2491	0.30	3.94	3.32	1.51
C11	0.179	2.22	2.71	0.020	3908	2286	0.87	0.24	2.88	1.85	1.16	3615	1902	0.31	2.10	1.83	0.80
C12	0.178	2.24	2.72	0.029	3918	2318	0.88	0.23	2.96	1.83	1.20	3644	1952	0.30	2.21	1.83	0.85
C13	0.142	2.32	2.70	0.010	4569	2634	1.06	0.25	4.02	2.70	1.61	4423	2303	0.31	3.23	2.89	1.23
C14	0.168	2.30	2.77	0.072	4310	2512	0.99	0.24	3.61	2.34	1.45	4128	2051	0.34	2.59	2.63	0.97
C15	0.341	1.70	2.58	0.060	2834	1605	0.48	0.26	1.11	0.78	0.44	2810	1332	0.36	0.82	0.94	0.30
C16	0.323	1.78	2.63	0.023	2864	1748	0.51	0.20	1.31	0.73	0.54	2774	1396	0.33	0.92	0.91	0.35
C17	0.318	1.80	2.64	0.030	2897	1727	0.52	0.22	1.32	0.80	0.54	2712	1326	0.34	0.85	0.90	0.32
C18	0.306	1.82	2.62	0.028	2947	1734	0.54	0.24	1.35	0.85	0.55	2788	1372	0.34	0.92	0.96	0.34
C19	0.267	1.96	2.68	0.051	3093	1928	0.61	0.18	1.72	0.90	0.73	2741	1274	0.36	0.87	1.05	0.32
C20	0.263	1.98	2.69	0.023	3236	1868	0.64	0.25	1.73	1.16	0.69	2914	1320	0.37	0.95	1.22	0.35
C21	0.234	2.06	2.68	0.067	3150	1915	0.65	0.21	1.82	1.03	0.75	2759	1415	0.32	1.09	1.02	0.41
Min	0.02	1.70	2.58	0.004	2834	1605	0.48	0.18	1.11	0.73	0.44	2712	1274	0.28	0.82	0.90	0.30
Max	0.34	2.77	2.83	0.075	6135	3429	1.70	0.29	8.28	6.09	3.25	6353	3241	0.37	7.70	7.29	2.91
Avg	0.18	2.21	2.71	0.031	4080	2354	0.93	0.24	3.38	2.32	1.35	3999	2018	0.33	2.79	2.68	1.05

$\phi$  = porosity (%);  $\rho_b$  = bulk density ( $g/cm^3$ );  $\rho_{ma}$  = matrix density ( $g/cm^3$ );  $K$  = permeability (mD);  $V_p$  = primary wave velocity (m/s);  $V_s$  = secondary wave velocity (m/s); A.I. = Acoustic impedance ( $*10^7$  kg/m<sup>2</sup>.s);  $\nu$  = Poisson's ratio;  $E$  = Young's modulus;  $\kappa$  = bulk modulus;  $\mu$  = shear modulus (the three elastic moduli are the given values times  $10^{10}$  N/m<sup>2</sup>). The suffix 'sat' denotes the acoustic properties of the water-saturated samples. Two samples (C2 and C3) are almost impermeable.

**Table 3.** Correlation coefficients (shown as  $r$  values) between the different petrophysical and acoustic parameters. Symbols and units are as explained in Table 2.

Physical Property	$\phi$	$\rho_b$	$\rho_{ma}$	K	Vp	Vs	A.I.	v	E	$\kappa$	$\mu$	Vp sat	Vs sat	v sat	E sat	$\kappa$ sat	$\mu$ sat
$\phi$	1																
$\rho_b$	-0.99	1															
$\rho_{ma}$	-0.87	0.91	1														
K	0.63	-0.51	-0.18	1													
Vp	-0.97	0.97	0.88	-0.53	1												
Vs	-0.97	0.98	0.91	-0.50	0.99	1											
A.I.	-0.97	0.99	0.90	-0.54	0.99	0.99	1										
v	-0.66	0.66	0.43	-0.37	0.70	0.63	0.72	1									
E	-0.93	0.99	0.92	-0.55	0.99	0.99	0.99	0.69	1								
$\kappa$	-0.92	0.99	0.90	-0.56	0.99	0.99	0.99	0.76	0.99	1							
$\mu$	-0.94	0.99	0.92	-0.54	0.99	0.99	0.99	0.68	0.99	0.99	1						
Vp sat	-0.95	0.95	0.79	-0.63	0.97	0.95	0.97	0.80	0.96	0.98	0.95	1					
Vs sat	-0.96	0.96	0.81	-0.58	0.98	0.96	0.98	0.77	0.97	0.98	0.97	0.99	1				
v sat	0.39	-0.42	-0.41	-0.10	-0.43	-0.45	-0.42	-0.33	-0.43	-0.25	-0.43	-0.31	-0.46	1			
E sat	-0.92	0.99	0.85	-0.62	0.99	0.97	0.98	0.78	0.98	0.99	0.97	0.99	0.99	0.43	1		
$\kappa$ sat	-0.91	0.96	0.81	-0.66	0.97	0.95	0.97	0.81	0.96	0.98	0.96	0.99	0.98	0.30	0.98	1	
$\mu$ sat	-0.92	0.99	0.85	-0.61	0.99	0.97	0.98	0.78	0.98	0.99	0.97	0.99	0.99	-0.45	0.99	0.98	1